A Facile Strategy of Boosting Photothermal Conversion Efficiency through States Transformation for Cancer Therapy

Jie Li[a], Jianxing Wang[a], Jianyu Zhang[b], Ting Han[a,*], Xiyao Hu[a], Michelle M. S. Lee[b], Dong Wang[a,*], Ben Zhong Tang[c,*]

[a] Center for AIE Research, Shenzhen Key Laboratory of Polymer Science and Technology, Guangdong Research Center for Interfacial Engineering of Functional Materials, College of Materials Science and Engineering, Shenzhen University, Shenzhen 518060, China.

[b] Hong Kong Branch of Chinese National Engineering Research Center for Tissue Restoration and Reconstruction, Department of Chemistry, The Hong Kong University of Science and Technology, Clear Water Bay, Kowloon, Hong Kong, China.

[c] Shenzhen Institute of Aggregate Science and Technology, School of Science and Engineering, The Chinese University of Hong Kong, Shenzhen, Guangdong 518172, China

Corresponding authors: hanting@szu.edu.cn, wangd@szu.edu.cn, tangbenz@cuhk.edu.cn

Abstract

Improving photothermal conversion efficiency (PCE) is critical to facilitate therapeutic performance during photothermal therapy (PTT). However, current strategies of prompting PCE always involve complex synthesis or modification of photothermal agents, thereby significantly inhibiting the practical applications and fundamental understanding of photothermal conversion. We herein present a facile strategy of transforming photothermal agents from aggregated state to dispersed state for boosting PCE. Compared to aggregated state, photothermal agents could rotate freely in dispersed state, allowing for an efficient non-radiative dissipation owing to twisted intramolecular charge transfer (TICT) effect. As the molecular motions are completely liberated in this strategy, the PCE enhancement is more remarkable than common methods of supporting molecular motions in aggregates. Noteworthy, this state transformation could be achieved in virtue of a releasing process from nanoparticles in lysosome of cancer cells, demonstrating a distinct photothermal therapeutic performance for cancer ablation. We hope this strategy of transforming state to boost PCE would be a new platform for practical applications of PTT technique.

Introduction

Photothermal therapy (PTT) has emerged as a promising method for tumor therapy, which absorb light to generate hyperthermia in tumor tissues, causing subsequent apoptosis or death of tumor cells.[1-6] In this field, of particular interest is organic photothermal agents (OPTAs) by virtue of their low toxicity, flexible modification, desirable biocompatibility and biodegradability.[7-11] To obtain desirable therapeutic performance, OPTAs are required with high photothermal conversion efficiency (PCE). Such high PCE could not only raise the possibilities to achieve hyperthermia above 50 °C for complete tumor ablation, but also reduce irradiation intensity to avoid the risk of damaging healthy skins and surrounding tissues.[12-14]

In principle, heat production heavily relies on non-radiative dissipation, which is absolutely competitive with radiative decay that accompanies by luminescence.[15-16] Therefore, the common strategies to boost PCE are diminishing radiative pathways or opening new avenues for non-radiative dissipation.[17-23] For example, Pu and co-workers encapsuled fullerenes to quench the fluorescence emission of nanoparticles (NPs) through intramolecular photoinduced electron transfer effect, where non-radiative decay dominated the energy dissipation and PCE was distinctly amplified.[24] Peng and co-workers modified a molecular rotor into the skeleton of OPTAs to promote non-radiative decay.[25] This motor can rotate in the core of NPs without energy barrier, rendering the PCE up to 88%. Although these provide insightful protocols for PCE enhancement, elaborated design and complex synthesis to OPTAs are normally involved, which significantly hindered the practical applications. Moreover, the modified substituents change the photochemical characteristics of OPTAs, impeding the insights into photothermal conversion mechanisms. Therefore, exploring simple strategy to boost PCE is of vital importance.

Fluorophores with distorted electron donor (D) - acceptor (A) structure possess the intrinsic feature of dissipating the excited-state energy through non-radiative relaxation by formation of a dark twisted intramolecular charge transfer (TICT) state.[26-28] This feature

potentially enables excellent photothermal performance. However, they usually exhibit inferior photothermal efficiency when used for *in vivo* application, because OPTAs are generally encapsulated in NPs, in which the intense aggregation dramatically hinders the intramolecular rotations, limiting the formation of TICT state but emitting bright fluorescence resulting from aggregation-induced emission (AIE) effect.[29-34] Recently, we have demonstrated that introducing branch-alkyl chains or bulky substrates could support the intramolecular motions in aggregates.[16,18,35-37] Nevertheless, the heat generation was not obviously elevated, as the motions were inevitably constrained in aggregated states. In this regard, we hypothesize that transforming OPTAs from aggregated to dispersed state could completely liberate the intramolecular motions, which would facilitate TICT formation to the greatest extent and produce an ultra-efficiently nonradiative pathways to maximize the conversion of light into heat.

Herein, we present a facile strategy to boost PCE by releasing OPTAs (BTPPA) from NPs to achieve the state transformation. As shown in Scheme 1, BTPPA NPs were prepared through co-assembly of BTPPA and amphiphilic copolymer PAE. As BTPPA stacked intensely in NPs (aggregated state), these NPs showed mild photothermal performance. After released form NPs, BTPPA transformed into dispersed state with free rotation, which drastically improved the formation of TICT state and thus remarkably promoted photothermal property. Importantly, owing to the acidic condition of lysosome-induced disassembly of NPs, the release behaviors and PCE enhancement could occur in tumors tissues, which tremendously improved therapeutic performance and simultaneously reduced the risk of damaging normal tissues. The strategy of transforming state to boost PCE is more flexible and efficient than traditional methods that involved tedious synthesis or modification, and we hope that this strategy would make a great contribution to fundamental understanding and practical application of PTT technique.
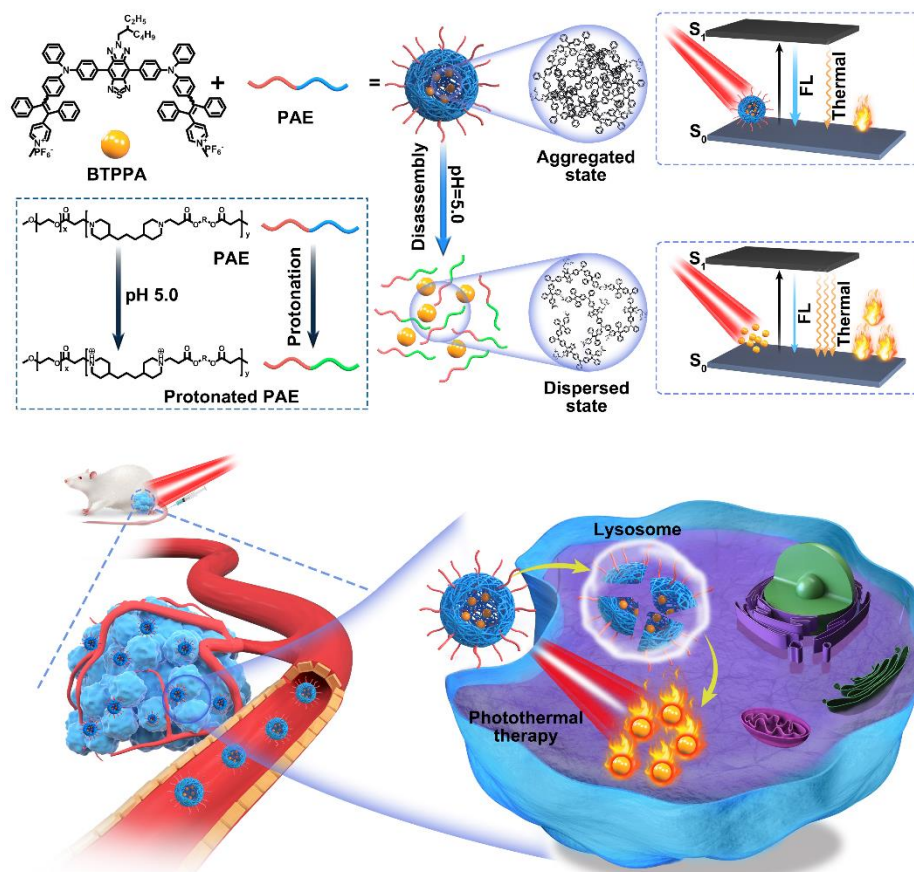
Scheme 1. Schematic illustration of state transformation of BTPPA to boost the PCE and the application for tumor photothermal therapy. FL: fluorescence.

Result and Discussion

To thoroughly confirm our assumption, three analogs with different substituted moieties (BTPAA, BTPEA and BTPPA) were designed and synthesized (Scheme S1-S3). As depicted in Fig. 1A, these molecules possessed conjugated D-A structures, in which benzotriazolethiadiazole (BTT) segment and triphenylamine (TPA) derivates served as strong electron acceptor and donor units, respectively. Density functional theory (DFT) calculation in Figure S1 clearly demonstrated the highest occupied molecular orbital (HOMO) of these molecules was delocalized along the conjugated backbone, while the lowest unoccupied molecular orbital (LUMO) was mainly located on the acceptor units. Such spatial separation

enabled small energy gaps between HOMO and LUMO, indicating the long absorbance and emission. UV/Vis and fluorescence spectra showed that these three molecules had maximum absorption wavelengths of ~ 600 nm (Fig. 1B), while the emission spectra were peaked at ~760 nm (Fig. 1C). Long wavelengths can deeply penetrate tissue and cause less tissue damage than UV or visible light, thus providing significant opportunity for biological applications. Moreover, optimized conformation calculations in Figure 1A reflected that these three molecules adopted highly twisted configurations in isolated states with large dihedral angles (~ 30°) between BTT and TPA units, which allowed TPA units to freely rotate, prompting the formation of TICT state.

Subsequently, the TICT properties of these molecules were studied. These molecules exhibited faint emission in polar solvent DMF, while the fluorescent intensity gradually increased with a blue shift after stepwise decreasing the polarity of solvent by adding toluene (Fig S2), solidly indicating their TICT effect. Moreover, with the increase of solvent polarity, the absorption wavelengths of three molecules varied slightly, whereas the maximum emissions underwent remarkable redshifts (Fig 2D and S3). For example, the emission wavelength of BTPEA was 744 nm in toluene, and it centered at 768 nm, 788 nm and 800 nm when in $CHCl_3$, DMF and DMSO, respectively, which can be ascribed to the intramolecular charge transfer (ICT) process. The quantitative analysis based on Lippert-Mataga equation further demonstrated that these three molecules possessed large difference on dipole moment between the ground and excited states (Fig 2E), suggesting the extraordinary strong TICT properties.[38-39]

The aggregated behaviors of these molecules were then investigated. BTPPA well dissolved in acetone and showed weak emission. After the addition of poor solvent ACN, the fluorescence intensities slightly increased with formation of aggregates, which indicated the typical AIE effect. Meanwhile, DMF was good solvent and water was poor solvent in BTPEA (Fig 1F and 1G) or BTPAA (Fig S4) systems. When increasingly added water into DMF

solution of BTPEA or BTPAA, the emission intensity reduced with redshifts at low water fractions, resulting from the TICT effect. At high water fractions, the intensity gradually increased with blueshifts. This was because BTPEA and BTPPA were in aggregated states and steric hindrance restrained the molecular motions, resulting in dominated pathways of radiative decay. These results demonstrated that three molecules were in isolated states in good solvent while in aggregated states upon exposure to poor solvents.
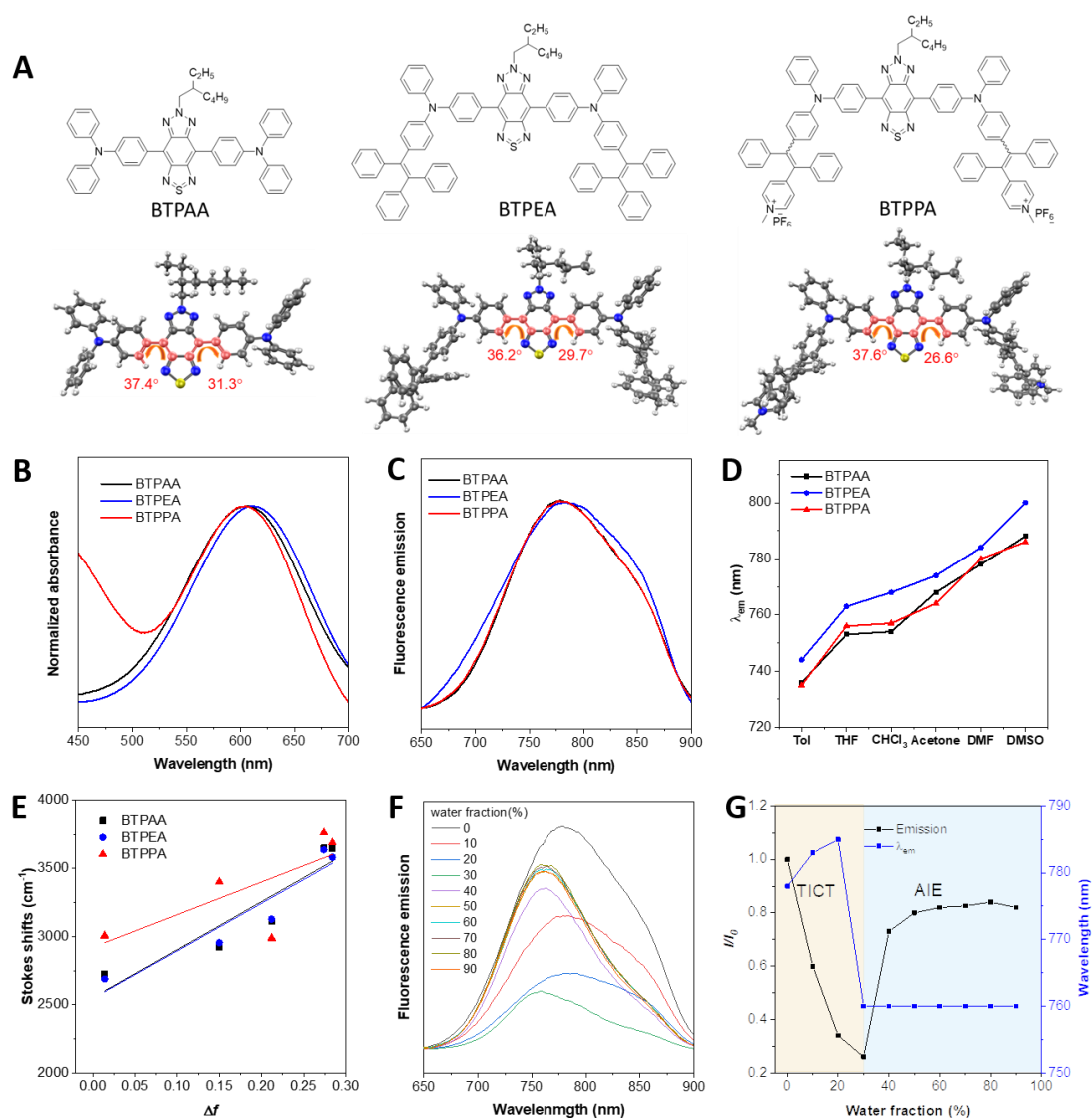

Figure 1. (A) Chemical structures and calculated optimized ground state (S_0) geometries of BTPAA, BTPEA and BTPPA. (B) Normalized absorbance and (C) fluorescence emission of these molecules in DMF. (D) Maximum emission wavelength in various solvents. (E) Correlation of Stokes shift *via* solvent polarity. (F) Fluorescence emission and (G) variations between fluorescence intensity and maximum

emission wavelength of BTPEA in DMF with different water fractions. [BTPAA] = [BTPEA] = [BTPPA] = 10 μM.

Next, the photothermal performances between dispersed and aggregated states were monitored. As shown in Figure 2A, the temperature remarkably increased under 660 nm laser irradiation (0.3 W/cm^2), and high temperature over 50 °C was observed within 300 s. Moreover, the maximum temperature was positively correlated to the irradiation intensities and concentrations of BTPPA, BTPEA and BTPAA (Fig S5). These outcomes indicated the excellent photothermal conversion properties. Owing to good solubility in DMF or acetone, these molecules were highly dispersed, while were in aggregated states upon exposure to exposed to poor solutions water or ACN. Fig 2B showed that the temperatures in dispersed state upon irradiation were much higher than these in aggregated states, and the PCEs of dispersed states were also larger than aggregated states (Fig 2C and S6). For example, the temperature of BTPEA in DMF solution reached to 52 °C after 5 min irradiation with a PCE of 52 %, while the temperature was only 38°C in water/DMF (v/v, 90:10) mixture under same condition, and the PCE reduced to 37%. These results solidly demonstrated that dispersed state hold better photothermal properties than aggregated state.
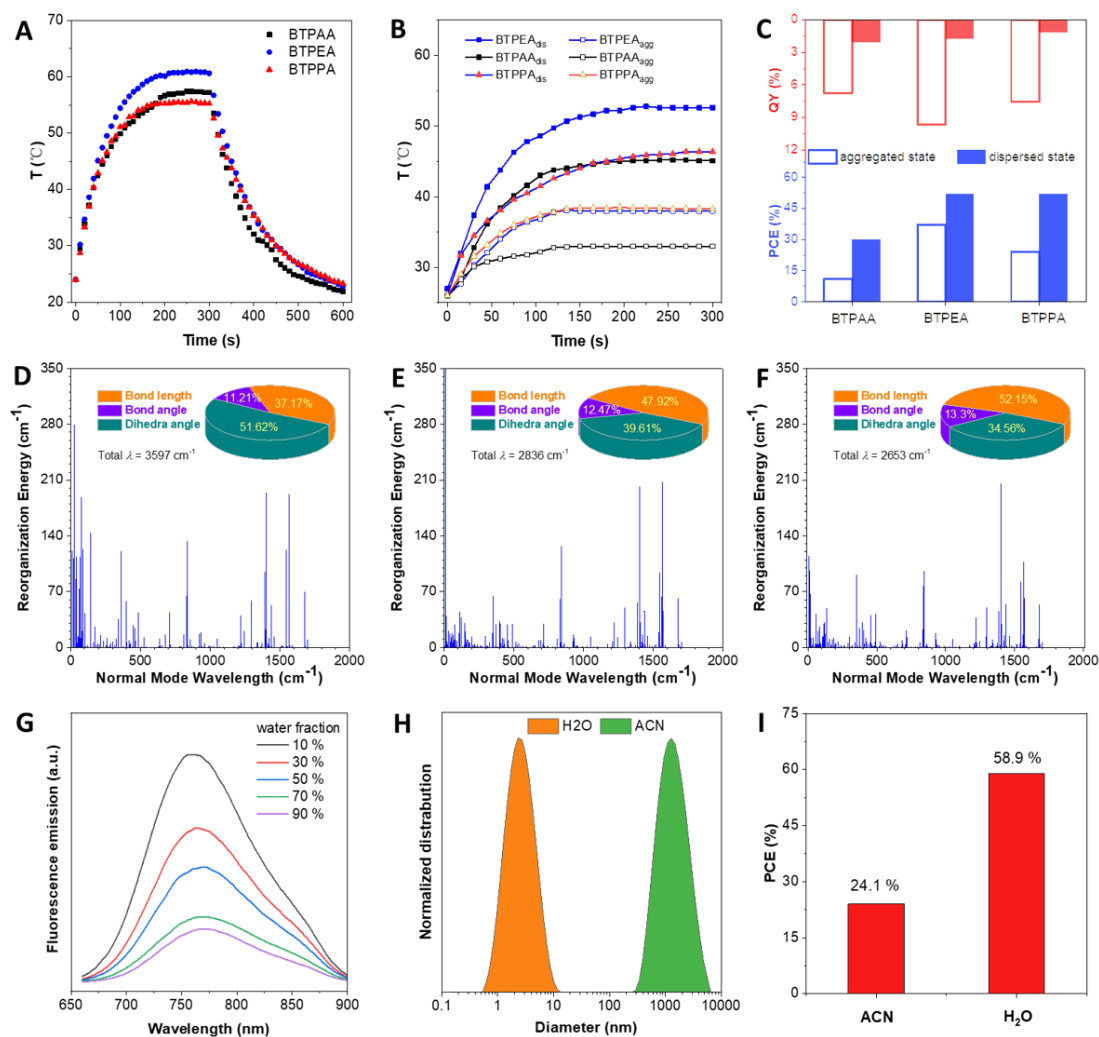
Figure 2. (A) Photothermal properties of BTPAA, BTPEA and BTPPA (150 μM) in DMF. (B) Photothermal properties of these molecules (100 μM) in aggregated state and dispersed state. (C) PCE and QY of these molecules in aggregated and dispersed state. Calculated reorganization energy and Contribution to the total reorganization energy of (D) BTPAA, (E) BTPEA and (F) BTPPA. (G) Fluorescence emission of BTPPA in ACN with different water fractions. (H) DLS results and (I) PCE of BTPPA in ACN and ACN/water (v/v, 10: 90) solutions.

To obtain deep insights into the difference of photothermal performances between two states, DFT calculation on reorganization energy was conducted. As depicted in Figure 2D, the main molecular motions of these molecules in free state were low frequency vibration modes, which were dynamic twisting motions and stretching of bonds. These two kinds of motions

made significant contributions to non-radiative decay pathways, enabling a rapid dissipation for excited energy to generate heat (Fig S7).[40] Therefore, these molecules exhibited promising photothermal efficiency in dispersed state. On the contrary, the compacted stacking in the aggregated state largely hindered intermolecular interactions, inhibiting the non-radiative channels and opening radiative decay pathways to emit bright fluorescence with high quantum yield (QY) but low PCE (Fig 2C).

Notably, as containing two hydrophilic pyridiniums, BTPPA had good water-solubility, providing potentials to form dispersed states in water. The ACN solution of BTPPA in the form of nanoaggregates with a diameter of 1500 nm showed intensive fluorescence emission (Fig S8). However, the emission intensity gradually reduced with increased water fractions (Fig 2G), where the nanoaggregates were declined to 2 nm when the water fraction was 90% (Fig 2H and S8). Moreover, compared with ACN solution, the PCE of BTPPA in water/ACN mixture was distinctly boosted from 24.1% to 58.9%, despite the generated temperature in water/ACN mixture was lower than ACN solution under the same irradiation conditions, suggesting the outstanding photothermal performance (Fig 2I and S9). The lower temperature in mixture can be ascribed to larger specific heat capacity of water than ACN.

To make use of the high PCE of BTPPA in biosystems, it was required to release BTPPA from NPs to achieve the dispersed state. As the most important organelle of cells, lysosome normally took in NPs through endocytosis and their acidic environment always served as stimuli to trigger NPs to release the loaded drugs or dyes.[41-44] Therefore, a pH-responsive polymer PEG-Poly(β-amino ester)$_6$ (PAE) was selected in this contribution. As shown in Scheme 1, this polymer self-assembled into NPs in physiological (pH~7.4) condition, and underwent a disassembly process upon exposed to acidic microenvironment of lysosomes (pH ~5) by reason that protonation of piperidine segments enhanced the hydrophilicity of polymers.[45,46] The BTPPA loaded NPs were prepared through a nanoprecipitation approach. UV/vis spectra clearly demonstrated that maximum absorbance of PAE NPs was 620 nm, and

the absorbance extended to 800 nm, which suggested these NPs can be irradiated by NIR laser (Fig 3A). DLS and TEM showed that the PAE NPs were spheres with a diameter of ~134 nm (Fig 3B). Zeta potential of PAE NPs was measured to be -10 mV (Fig S10). These results suggested that PAE NPs were favorable for tumor accumulation through enhanced-permeability-and-retention (EPR) effect.

When PAE NPs were in acidic solution of pH = 5.0 (acidic microenvironment of lysosome), their Zeta potentials drastically changed and increased to 20 mV, indicating the protonation of piperidine segments. Moreover, no aggregate was observed in TEM (Fig S11), which reflected the disassembly of NPs at this condition. Significantly, Figure 3C demonstrated that BTPPA was rapidly released from NPs in pH = 5 solution and the released fraction reached to 82% within 10 hours. In contrast, the released fraction was as low as 18% in pH = 7.4 solution. Such obvious difference strongly demonstrated the acidic condition-triggered release of BTPPA. As a control, when BTPPA was loaded in PEG NPs, which were prepared by the PEG-COOH polymer without pH-responsive property, the released fractions were quite low in both pH = 7.4 (9%) and 5.0 (16%), and the sizes, morphologies and Zeta potentials of PEG NPs seldom changed (Fig S12 and S13), revealing the insignificant release of BTPPA from PEG NPs. These results showed that PAE NPs were ideal carriers to release loaded BTPPA in acidic condition through disassembly process.

The photothermal properties in different pH solutions were detected as well. It was observed that the generated temperature was both concentration- and the laser intensity-depended (Fig S14). As depicted in Figure 3E, the temperature of PAE NPs in pH = 7.4 solution shapely increased from 28 °C to 47 °C within 5 min under 660 nm laser irradiation. Excitingly, the temperature reached to 65 °C at the same conditions when the pH was 5.0, and the corresponding PCE was calculated to be 60 %, which was quite higher than 43% in pH = 7.4 (Fig S15). Thermal images in Figure 3F directly demonstrated the distinct difference on photothermal properties. The higher temperature and better PCE in acidic solution than neutral

solutions were attributed to disassembly of PAE NPs, in which numerous moieties of BTPPA could freely rotate. The PL spectra (Fig 3D) and lifetime results (Fig S10) showed that the emission was remarkably deceased with a redshift and the lifetime drastically shortened from 1.6 to 0.06 ns when pH changed from 7.4 to 5.0, verifying the dispersed state in acidic solution. Oppositely, PEG NP exhibited low temperature, low PCE, strong fluorescence emission and long lifetime in each solution with pH values of 7.4 or 5.0, mainly because PEG NPs remained the same morphology without the release of BTPPA molecules.
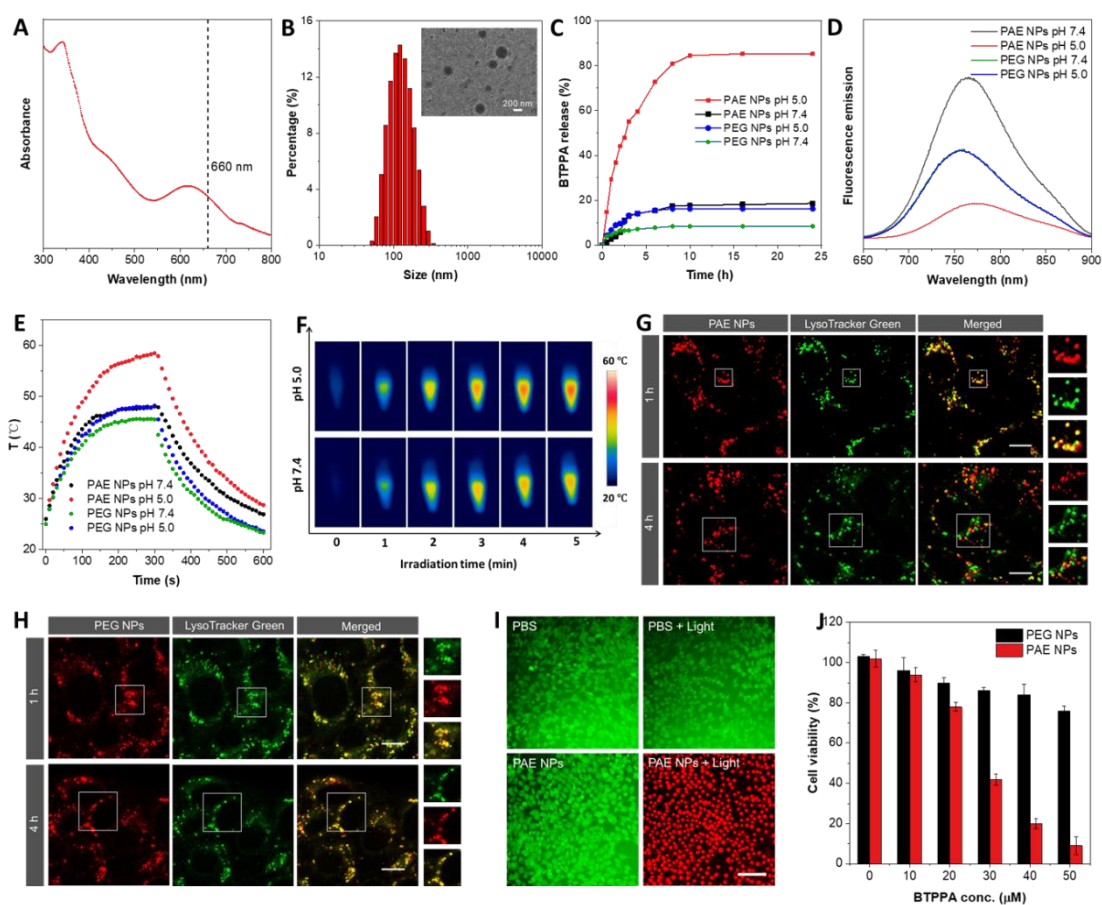

Figure 3. (A) Absorbance and (B) DLS distribution of BTPPA loaded PAE NPs in water. Inset: TEM image of PAE NPs. (C) BTPPA release profile, (D) fluorescence emission and (E) photothermal properties of PAE NPs and PEG NPs (200 μM) at different pH conditions. (F) Real-time thermal images of BTPPA loaded PAE NPs (200 μM) at different pH solution under 660 nm laser irradiation (0.3 W/cm^2). Co-location images of 4TI cells after incubated with PAE NPs (G) and PEG NPs (H) with different periods. scale bar: 10 μm. (I) Live/dead cell co-staining fluorescence imaging of 4T1 cells with different

treatments. scale bar: 100 μm. (J) Cell viability of 4T1 cells incubated with PAE and PEG NPs at various

concentrations in the dark and after 660 nm laser irradiation (0.3 W/cm², 5 min).

The release behavior and phototherapeutic efficiencies were further conducted using 4T1

cell as model. When incubated with BTPPA loaded PAE NPs and PEG NPs, obvious red signal

was detected in 4T1 cells, and the signal intensity continually enhanced over time (Fig S16),

which indicated that both NPs successfully entered 4T1 cells. Moreover, co-location imaging

(Fig 3G, 3H and S17) showed that the red emissions from NPs were perfectly overlapped with

the green signal of lysosome probe after a period of 1 h incubation, demonstrating the

endocytosis by lysosomes. Importantly, with further increasing the incubated time to 4 hours,

most of the red signal in PAE NPs system distributed in cytoplasm, whereas the red emission

of PEG NPs remained in lysosomes, suggesting the disassembly of PAE NPs and releasing of

BTPPA in lysosome. Furthermore, both PAE NPs and PEG NPs exhibited negligible toxicity

to cancer cell in the dark, making them suitable and safe for bio-application (Fig S18). However,

upon irradiation with 660 nm laser, the cell viability of PAE NPs rapidly decreased over

concentrations (Fig 3J). Notably, the cell viability of PAE NPs was remarkably lower than PEG

NPs at the same concentration. For example, when the concentration of BTPPA was 50 μM, in

the case of PAE NPs, the cellular viability of was only 10% upon laser irradiation, which was

remarkably lower than that of PEG NPs (78%). This outcome strongly revealed the fantastic

phototherapeutic efficiency of PAE NPs for cancer cells, which was ascribed to the

extraordinarily better photothermal performance of BTPPA in dispersed state than aggregated

state in PEG NPs. To demonstrate phototherapeutic effect of PAE NPs intuitively, a fluorescein

diacetate/propidium iodide (FDA/PI) double staining protocol was utilized to distinguish live

(green) and dead (red) 4T1 cells. As depicted in Fig 3I, 4T1 cells exhibited green fluorescence

when treated with PBS or PAE NPs without irradiation, manifesting low side effect of the laser

dosage and good biocompatibility of NPs, while the cells were completely eliminated, showing

red emission after incubated with PAE NPs under irradiation. In addition, dichlorodihydrofluorescein diacetate (DCFH-DA) was employed as reactie oxygen species (ROS) indicator to evaluate the photodynamic effect of PAE NPs. The NPs showed a weaker ROS generation in acidic condition than pH = 7.4 (Fig S19). Taken together, these results solidly demonstrated that BTPPA in dispersed state had extraordinarily better phototherapeutic efficiency than aggregated state.

In vivo fluorescence imaging and phototherapeutics outputs of PAE NPs were investigated in 4T1 tumor-bearing mice and PEG NPs were used as a control. After intravenous injection of both NPs for 2 hours, bright emission can be observed in tumor and the emission intensities gradually increased with prolonged time, indicating the excellent accumulation of NPs in tumor tissue (Fig S20). At 8 hours postinjection, the intensity reached the maximum, and NPs were mainly distributed in tumors according to *ex vivo* organ images, suggesting the optimal treatment time for irradiation. Importantly, the tumor tissues in PAE NPs group exhibited a much weaker fluorescence signals than PEG NPs group at same periods. This was because the dispersed state was formed in PAE NPs group with low QY, while BTPPA was in aggregated state in PEG NPs, showing the bright fluorescence emission. The photothermal properties were also recorded through real-time temperatures of tumors. As shown in Figure 4A and 4B, after irradiating with 660 nm laser (0.3 W cm^{-2}) for 5 min, the tumor temperatures shapely increased from 37 to 52 °C within 3 min when injected with PAE NPs. In comparison, the temperatures only raised to 45 °C after treated with PEG NPs, and negligible temperature variation was observed in saline-administrated mouse. This revealed that BTPPA in dispersed sates had promising photothermal conversion for *in vivo* applications.
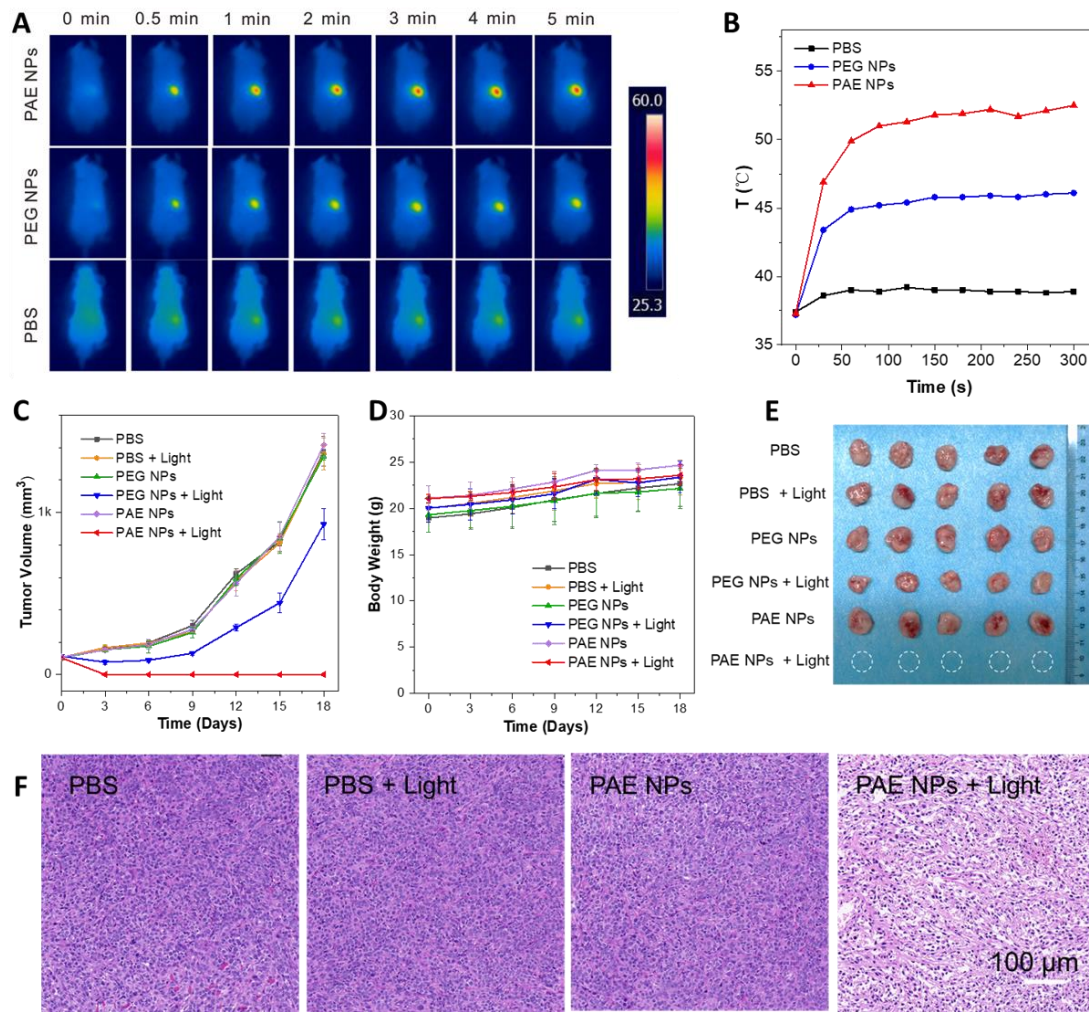
Figure 4. (A) IR thermal images and (B) temperature change of 4T1 tumor-bearing nude mice after intravenous injection of PAE NPs, PEG NPs or PBS under 660 nm laser irradiation (0.3 W/cm^2) for 5 min. (C) Tumor sizes and (D) bodyweights of mice with different treatments. (E) Photograph for tumors retrieved from mice after 18 days (dashed cycle indicate eliminated tumors). (F) H&E analysis of tumor tissues with different treatments.

To comprehensively monitor the *in vivo* phototherapeutic efficiency, 4T1 tumor-bearing nude mice were randomly divided into six groups: (1) PBS, (2) PBS + Light, (3) PEG NPs , (4) PEG NPs + Light, (5) PAE NPs and (6) PAE NPs + Light. The light irradiation groups underwent once irradiation (660 nm, 0.3 W cm^{-2}, 10 min) at 8-hours postinjection. Figure 4C and S21 showed that the tumors of all dark groups and PBS groups rapidly grew and the tumor

sizes of each group did not have obvious difference, indicating that only laser irradiation or NPs had negligible efficiency for cancer therapy. Noteworthy, the tumors in "PAE NPs + light" group were completely ablated at the third day after irradiation, leaving burned scars on the tumor sites. The scars gradually disappeared and the tumors were eliminated without recurrence during the subsequent 15 days, solidly demonstrating the fantastic therapeutic performance to tumors (Fig 4E). The tumors volumes of "PEG NPs + light" group did not increase within 6 days, but then quickly expanded and generated large tumors at 18 days because of the incomplete tumor ablation, resulting from the insufficient photothermal conversion of PEG NPs. Moreover, hematoxylin and eosin (H&E) staining of tumor slices revealed that PAE NPs caused obvious damages to tumor tissues with many void spaces under laser irradiation (Fig 4F).

Finally, the physiological safety of PAE NPs was examined. No significant body weight loss was found in all tested groups, implying that PAE NPs did not trigger obvious toxicity to mice (Fig 4D). Moreover, blood routine analysis of healthy mice treated with PAE NPs demonstrated that all the parameters were at normal levels, verifying the good biocompatibility (Table S1). Furthermore, the histological evaluation by the H&E staining showed that the major organs (heart, liver, spleen, lung, and kidney) were not damaged after treated with NPs, suggesting the excellent safety to mice (Figure S22). Therefore, it was concluded that PAE NPs had high biological compatibility and safety, and hold promising potentials for *in vivo* photothermal applications.

Conclusion

In summary, we developed a facile strategy to boost photothermal performance by stimuli-responsive stacking state transformation of AIE-active photothermal agents, reaching up to 60% of photothermal conversion efficiency. In aggregation state, the compact stacking restrained the intramolecular motions, allowing for efficient radiative decay pathways with bright emission. In contrast, photothermal agent adopted twisted structure and rotated freely in

molecularly dissolved state, opening non-radiative channel for energy dissipation with high photothermal conversion performance. Noteworthy, *in vitro* and *in vivo* experiments demonstrated that the state transformation occurred in lysosome in virtue of acidic condition-induced disassembly of NPs. As a result, the released photothermal agent exhibited fantastic antitumor therapeutic efficiency, affording complete tumor elimination with only once injection and a single irradiation. This successful example of photothermal agent design could prompt the practical application of photothermal therapy technique.

Supporting information

The supporting information can be found in XXX.

Conflict of Interest

The authors declare no conflict of interest.

Reference

1. Y. Liu, P. Bhattarai, Z. Dai, X. Chen, *Chem. Soc. Rev.* **2019**, *48*, 2053.

2. H. S. Jung, P. Verwilst, A. Sharma, J. Shin, J. L. Sessler, J. S. Kim, *Chem. Soc. Rev.* **2018**, *47*, 2280.

3. Y. Liu, H. Wang, S. Li, C. Chen, L. Xu, P. Huang, F. Liu, Y. Su, M. Qi, C. Yu, Y.

Zhou, *Nat Commun.* **2020**, *11*, 1724.

4. X. Yi, H. Zhou, Y. Chao, S. Xiong, J. Zhong, Z. Chai, K. Yang, Z. Liu, *Sci. Adv.* **2020**, 6, 3546.

5. Q. Wang, H. Wang, Y. Yang, L. Jin, Y. Liu, Y. Wang, X. Yan, J. Xu, R. Gao, P. Lei, J. Zhu, Y. Wang, S. Song, H. Zhang, *Adv. Mater.* **2019**, *31*, 1904836.

6. L. Zhao, Y. Liu, R. Xing, X. Yan, *Angew. Chem. Int. Ed.* **2020**, *59*, 3793.

7. S. Gao, G. Wei, S. Zhang, B. Zheng, J. Xu, G. Chen, M. Li, S. Song, W. Fu, Z. Xiao, W. Lu, *Nat. Commun.* **2019**, *10*, 2206.

8. H. Zhou, X. Zeng, A. Li, W. Zhou, L. Tang, W. Hu, Q. Fan, X. Meng, H. Deng, L. Duan, Y. Li, Z. Deng, X. Hong, Y. Xiao, *Nat. Commun.* **2020**, *11*, 6183.

9. S. Li, Q. Deng, Y. Zhang, X. Li, G. Wen, X. Cui, Y. Wan, Y. Huang, J. Chen, Z. Liu, L. Wang, C.-S. Lee, *Adv. Mater.* **2020**, *32*, 2001146.

10. B. Qiao, Y. Luo, H.-B. Cheng, J. Ren, J. Cao, C. Yang, B. Liang, A. Yang, X. Yuan, J. Li, L. Deng, P. Li, H.-T. Ran, L. Hao, Z. Zhou, M. Li, Y. Zhang, Pe. S. Timashev, X.-J. Liang, Z. Wang, *ACS Nano* **2020**, *14*, 12652.

11. H. Xiang, L. Zhao, L. Yu, H. Chen, C. Wei, Y. Chen, Y. Zhao, *Nat. Commun.* **2021**, *12*, 218.

12. C. Xu, K. Pu, *Chem. Soc. Rev.* **2021**, *50*, 1111.

13. X. Zhen, C. Xie, K. Pu, *Angew. Chem. Int. Ed.* **2018**, *57*, 3938.

14. M. Su, Q. Han, X. Yan, Y. Liu, P. Luo, W. Zhai, Q. Zhang, L. Li, C. Li, *ACS Nano* **2021**, *15*, 5032.

15. G. Feng,a G.-Q. Zhang, D. Ding. *Chem. Soc. Rev.* **2020**, *49*, 8179.

16. S. Liu, X. Zhou, H. Zhang, H. Ou, J. W. Y. Lam, Y. Liu, L. Shi, D. Ding, B. Z. Tang, *J. Am. Chem. Soc.* **2019**, *141*, 5359.

17. D. Wang, M. M. S. Lee, W. Xu, G. Shan, X. Zheng, R. T. K. Kwok, J. W. Y. Lam, X. Hu, B. Z. Tang, *Angew. Chem. Int. Ed.* **2019**, *58*, 5628.

18. Z. Zhao, C. Chen, W. Wu, F. Wang, L. Du, X. Zhang, Y. Xiong, X. He, Y. Cai, R. T.K. Kwok, J. W.Y. Lam, X. Gao, P. Sun, D. L. Phillips, D. Ding, B. Z. Tang, *Nat. Commun.* **2019**, *10*, 768.

19. J.-S. Ni, X. Zhang, G. Yang, T. Kang, X. Lin, M. Zha, Y. Li, L. Wang, K. Li, *Angew. Chem. Int. Ed.* **2020**, *59*, 11298.

20. M. Chen, X. Zhang, J. Liu, F. Liu, R. Zhang, P. Wei, H. Feng, M. Tu, A. Qin, J. W. Y. Lam, D. Ding, B. Z. Tang, *ACS Nano* **2020,** *14*, 4265.

21. X. Mu, Y. Lu, F. Wu, Y. Wei, H. Ma, Y. Zhao, J. Sun, S. Liu, X. Zhou, Z. Li, *Adv. Mater.* **2020**, *32*, 1906711.

22. L. Zhao, Y. Liu, R. Chang, R. Xing, X. Yan, *Adv. Funct. Mater.* **2019**, *29*, 1806877.

23. B. Wang, G. Feng, M. Seifrid, M. Wang, B. Liu, G. C. Bazan, *Angew. Chem. Int. Ed.* **2017**, *56*, 16063.

24. Y. Lyu, Y. Fang, Q. Miao, X. Zhen, D. Ding, K. Pu, *ACS Nano* **2016**, *10*, 4472.

25. D. Xi, M. Xiao, J. Cao, L. Zhao, N. Xu, S. Long, J. Fan, K. Shao, W. Sun, X. Yan, X. Peng, *Adv. Mater.* **2020**, *32*, 1907855.

26. Z. R. Grabowski, K. Rotkiewicz, *Chem. Rev.* **2003**, *103*, 3899.

27. H. Dong, Y. Wei, W. Zhang, C. Wei, C. Zhang, J. Yao, Y. S. Zhao, *J. Am. Chem. Soc.* **2016**, *138*, 1118.

28. S. Sasaki, G. P. C. Drummen, G. Konishi, *J. Mater. Chem. C* **2016**, *4*, 2731.

29. T. Mori, H. Chin, K. Kawashima, H. T. Ngo, N.-J. Cho, W. Nakanishi, J. P. Hill, K. Ariga, *ACS Nano* **2019**, *13*, 2410.

30. J. Li, Y. Qian, L. Xie, Y. Yi, W. Li, W. Huang, *J. Phys. Chem. C* **2015**, *119*, 2133.

31. R. Hu, C. F. A. Go´mez-Dura´n, J. W. Y. Lam, Jose´ L. Belmonte-Va´zquez, C. Deng, S. Chen, R. Ye, E. Pen˜a-Cabrera, Y. Zhong, K. S. Wong, B. Z. Tang, *Chem. Commun.* **2012**, *48*, 10099.

32. K. Li, Y. Liu, Y. Li, Q. Feng, H. Hou, B. Z. Tang, *Chem. Sci.* **2017**, *8*, 7258.

33. C. Wang, Q. Qiao, W. Chi, J. Chen, W. Liu, D. Tan, S. McKechnie, D. Lyu, X.-F. Jiang, W. Zhou, N. Xu, Q. Zhang, Z. Xu, X. Liu, *Angew. Chem. Int. Ed.* **2020**, *59*, 10160.

34. J. Mei, Y. Hong, J. W. Y. Lam, A. Qin, Y. Tang, B. Z. Tang, *Adv. Mater.* **2014**, *26*, 5429.

35. S. Liu, Y. Li, R. T. K. Kwok, J. W. Y. Lam, B. Z. Tang, *Chem. Sci.* **2021**, *12*, 3427.

36. Y. Li, Z. Cai, S. Liu, H. Zhang, S. T.H. Wong, J. W.Y. Lam, R. T.K. Kwok, J. Qian, B. Z. Tang, *Nat. Commun.,* **2020**, *11*, 1255.

37. J. Wang, J. Li, L. Wang, T. Han, D. Wang, B. Z. Tang, *ACS Appl. Polym. Mater.* **2020**, *2*, 4306.

38. N. A. Sayresmith, A. Saminathan, J. K. Sailer, S. M. Patberg, K. Sandor, Y. Krishnan, M. G. Walter, *J. Am. Chem. Soc.* **2019**, *141*, 18780.

39. W. Li, D. Liu, F. Shen, D. Ma, Z. Wang, T. Feng, Y. Xu, B. Yang, Y. Ma, *Adv. Funct. Mater.* **2012**, *22*, 2797.

40. S. Liu, C. Chen, Y. Li, H. Zhang, J. Liu, R. Wang, S. T. H. Wong, J. W. Y. Lam, D. Ding, B. Z. Tang, *Adv. Funct. Mater.* **2020**, *30*, 1908125.

41. G. Liu, X. Zhao, Y. Zhang, J. Xu, J. Xu, Y. Li, H. Min, J. Shi, Y. Zhao, J. Wei, J. Wang, G. Nie, *Adv. Mater.* **2019**, *31*, 1900795.

42. T.-T. Chen, J.-T. Yi, Y.-Y. Zhao, X. Chu, *J. Am. Chem. Soc.* **2018**, *140*, 9912.

43. S. Wang, G. Yu, Z. Wang, O. Jacobson, R. Tian, L.-S Lin, F. Zhang, J. Wang, X. Chen, *Adv. Mater.* **2018**, *30*, 1803926.

44. P. Liang, X. Huang, Y. Wang, D. Chen, C. Ou, Q. Zhang, J. Shao, W. Huang, X. Dong, *ACS Nano* **2018**, *12*, 11446.

45. S. J. Hwang, M. S. Kim, J. K. Han, D. S. Lee, *Macromol. Res.* **2007**, *15*, 437.

46. K. H. Min, J.-H. Kim, S. M. Bae, H. Shin, M. S. Kim, S. Park, H. Lee, R.-W. Park, I.-S. Kim, K. Kim, I. C. Kwon, S. Y. Jeong, D. S. Lee, *J. Control. Release* **2020**, *144*, 259.